Gold-Nanoparticle-Assisted Laser Perturbation of Chromatin Assembly Reveals Unusual Aspects of Nuclear Architecture within Living Cells

Aprotim Mazumder* and G. V. Shivashankar*†
*National Centre for Biological Sciences, Tata Institute of Fundamental Research, and †Raman Research Institute, Bangalore, India

ABSTRACT Chromatin organization within the nucleus is a vital regulator of genome function, yet its mechanical coupling to the nuclear architecture has remained elusive. To directly investigate this coupling, we locally modulated chromatin structure in living cells using nanoparticle-based laser perturbation. Unusual differences in the response of the cell nucleus were observed depending on the nuclear region that was perturbed—the heterochromatin, the euchromatin, and the nuclear envelope. This response varied under different conditions of cellular perturbations such as ATP depletion, apoptosis, and inhibition of histone deacetylases. Our studies implicate heterochromatin organization in imparting mechanical stability to the cell nucleus and suggest that nuclear size and shape are the result of interplay between nuclear and cytoplasmic anchors.

INTRODUCTION

Chromatin assembly in the interphase cell nucleus is stabilized by histone tail interactions and other nuclear proteins into a highly organized and dynamic structure (1). This structural stability is known to be governed primarily by the nuclear membrane and the lamin network. The architectural organization of the interphase cell nucleus is a vital regulator of gene expression in eukaryotes. Confinement of chromosomes into relatively discrete chromosome territories, as well as biochemical and structural evidence for chromatin loops anchored to lamin networks, suggests that such tethers could impose order on nuclear organization (1–4). The positions of chromosomes in the nucleus are nonrandom and are preserved through mitosis (5), and this has been implicated in the maintenance of tissue-specific cellular memory (6). Furthermore, translocation of genes to active loci brought about by spatial reorganization of chromatin is emerging as a crucial mechanistic process to regulate transcription (7–9). Genomic DNA is condensed by histone and other nuclear proteins within the cell nucleus in the form of chromatin fibers. In interphase cells the chromatin is differentially packed into 1), predominantly silent, densely organized heterochromatin and 2), transcriptionally active, gene-rich, and comparatively more accessible euchromatin (10). It has been suggested that the nucleus is maintained under opposing forces resulting from cytoplasmic and nuclear elements (11). Thus, apart from the chromatin, mechanical stability is imparted to the nucleus by the inner and outer nuclear membranes and the nuclear lamina, perhaps connecting up to heterochromatin regions (12). The lamin proteins and associated proteins such as lamin B receptor (LBR, an inner nuclear membrane protein) have been shown to bind to dsDNA, core histones, heterochromatin protein HP-1, and chromatin-associated protein HA95, and disruption of these interactions leads to a variety of clinical disorders (13). Nuclear morphology has been shown to be directly related to the lifespan of an organism, from *Caenorhabditis elegans* (14) to humans (15). The long-term changes in cellular structure on perturbation likely reflect a mechanosignaling coupling between structure and signaling cascades, as seen before (16). Thus, the importance of cellular filaments and the chromatin assembly in maintaining nuclear architecture in normal cells and its alterations in cancerous cells (17) can hardly be overemphasized. Although a functional interplay of the chromatin, the nuclear envelope, and an underlying proteinaceous scaffold is expected, attempts at mechanistically probing these interactions remain few. Thus, to investigate the differential physical coupling of chromatin assembly to nuclear architecture, we employ the efficient absorption of gold nanoparticles to near-infrared (NIR) radiation as a method to produce controlled spatial perturbation of nuclear substructures within single living cells.

METHODS

Cell culture and incorporation of gold nanoparticles

HeLa cells were cultured in DMEM/F12 medium (Gibco, Grand Island, NY) supplemented with 5% fetal bovine serum (FBS) (Gibco) and penicillin-streptomycin (Gibco), in a 5% CO_2 incubator. HeLa WT cells were transfected using Lipofectamine 2000 (Invitrogen, Carlsbad, CA). Stable cell lines expressing H2B-EGFP were generated using selection by Blasticidin (Invitrogen). The ~5-nm gold particles were incorporated into HeLa cells by a hypotonic shock to the cells, a modification of the method presented by Koberna et al. (18). We found this method to be better for a widespread distribution of the particles to the cells, and it also is less damaging to the cells than microinjection. Briefly, HeLa cells grown on coverslip dishes for 2 d were preincubated with regular medium supplemented with the gold particles for 1 h to ensure the presence of the particles in the endocytosed fluid.

Submitted December 1, 2006, and accepted for publication May 7, 2007.

Address reprint requests to G. V. Shivashankar, National Centre for Biological Sciences, Tata Institute of Fundamental Research, Bellary Road, Bangalore 560065, India. E-mail: shiva@ncbs.res.in.

Editor: Stuart M. Lindsay.

0006-3495/07/09/2209/08 $2.00

doi: 10.1529/biophysj.106.102202

The cells were washed twice with phosphate-buffered saline (PBS), pH 7.4, and then given a hypotonic shock with the gold solution for 3 min at 37°C. The cells were gently washed and placed in phenol-red-free regular cell-culture medium and allowed to recover for 3–4 h before imaging and perturbation experiments.

Cellular perturbations

ATP depletion of cells was carried out by a treatment of the cells with 6 mM 2-deoxy-D-glucose and 10 mM sodium azide in glucose-free M1 buffer for 1 h at 37°C. Apoptosis was induced by treating the cells with 10 μM staurosporine in M1 buffer for 4 h at 37°C. Chromatin decondensation by HDAC inhibition was carried out by treatment of the cells with 200 ng/ml Trichostatin A (TSA) in cell culture medium for 4 h at 37°C. TSA was added 1 h after the hypotonic shock to the cells to incorporate gold particles.

Isolation of nuclei from HeLa cells and Preparation of chromatin samples

Freshly harvested H2B-EGFP HeLa cells were washed in PBS (pH 7.4) buffer and resuspended in TM2 buffer (10 mM Tris-HCl, pH 7.4, 2 mM $MgCl_2$, and 0.5 mM PMSF (added fresh before use)). The cells were incubated for 5 min each in room temperature and on ice. Then, 0.5% v/v of Triton-X100 was added and mixed thoroughly before incubation on ice for another 5 min. The cells were sheared by passing them through a syringe needle (22 gauge) a few times and centrifuged at 500 rpm for 5 min, to obtain nuclei. The nuclei were observed under the microscope, and Triton-X100 treatment was repeated if the nuclei were found to have cellular debris sticking to them. Clean isolated nuclei, completely free of cellular debris, were used for experiments, and all experiments were performed in PBS buffer at pH 7.4. Isolated nuclei were placed on poly-D-lysine-coated cover slips and imaged in M1 buffer in the temperture-controlled chamber. Gold nanoparticles were added to the medium to a high final concentration of 300 pM.

RESULTS

Differential response of distinct chromatin regions to nanoparticle-assisted laser perturbation

HeLa cells stably expressing the core histone H2B tagged to EGFP were incorporated with gold nanoparticles by a hypotonic shock to the cells. The biocompatibility and low cytotoxicity of the gold nanoparticles used have been well characterized (19). Local perturbation of chromatin assembly was achieved by heating up the gold nanoparticles by focusing an NIR beam at the desired spatial location with diffraction resolution. The gold particles increase the efficiency of absorption to NIR radiation producing local heating effects thereby allowing one to spatially address single cells and sub-cellular structures (Supplementary Fig. 1, *A–E*). From fluorescence intensity maps of histone H2B-EGFP, densely and loosely packed regions of the chromatin, corresponding to heterochromatin and euchromatin, were identified. These regions were perturbed with a 2.5-μm spot in the nuclei of gold-incorporated (GI) cells after exposure to a pulsed Ti-sapphire laser mode locked at 835 nm (56 mW at the sample plane at a single spot) for a period of ~3 s.

Perturbation at the dense regions such as perinucleolar heterochromatin invariably caused a dramatic shrinkage of the cell nucleus, although the loose euchromatin regions showed only marginal shrinkage (Fig. 1 *A*). The stark difference in response to perturbation probably indicates the differential coupling of the euchromatin and the heterochromatin to nuclear architecture. Shrinkage in the *XY* plane was usually

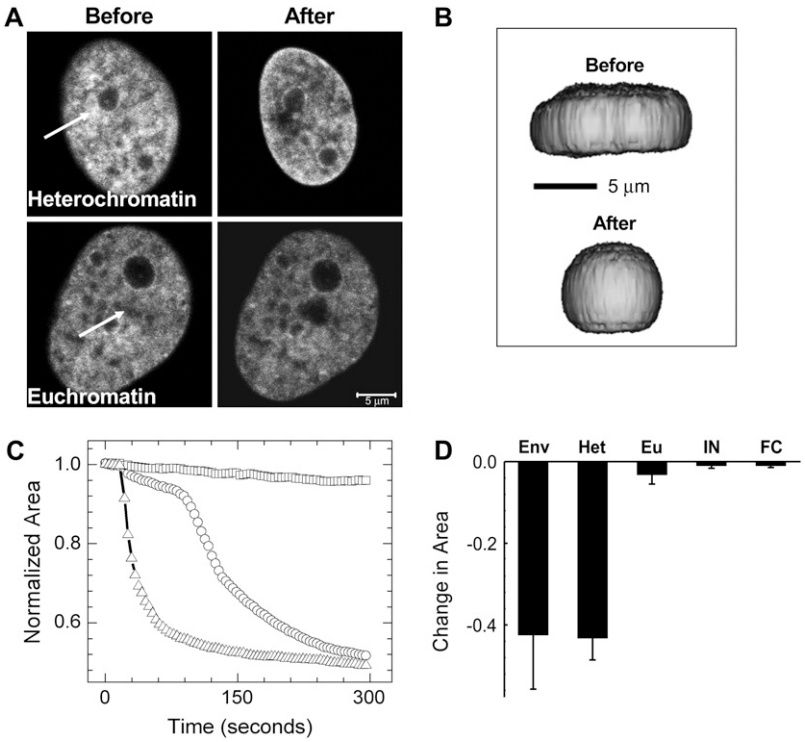

FIGURE 1 (*A*) Images before and after perturbation of heterochromatin and euchromatin in H2B-EGFP HeLa cells. The region indicated by the white arrows was exposed to ~3 s of 835-nm NIR radiation, and the effect was monitored by imaging the H2B-EGFP fluorescence with the 488-nm line of an argon ion laser. The scale bar is equal to 5 μm. (*B*) Three-dimensional reconstructions of a cell made from a *z*-stack of confocal slices before and after perturbation shown from a primarily *XZ* perspective. Note that shrinkage in the *XY* plane is accompanied by a slight expansion in *Z*. (*C*) Representative plots of shrinkage dynamics for perturbation at the nuclear envelope (*triangles*), heterochromatin (*circles*), and euchromatin (*squares*) (*D*) Statistics of fractional change in area for perturbation at the nuclear envelope (*Env*), heterochromatin (*Het*), and euchromatin (*Eu*) ($n = 12$). Standard deviations are plotted as error bars. Also shown are similar statistics for isolated nuclei (*IN*) and fixed cells (*FC*) ($n = 10$), which did not show any shrinkage dynamics.

accompanied by a slight expansion in the *Z* direction. This is depicted in Fig. 1 *B*. which shows the *XZ* profile of a cell before and after perturbation, reconstructed from confocal *z*-stacks in a typical experiment. This indicates an overall loss of shape anisotropy and, hence, a loss of lateral cytoplasmic tension. And as expected, there is a corresponding overall decrease in volume, indicating increased inward forces. We took confocal *z*-stacks of nuclei before and after perturbation and estimated nuclear volumes. The data from seven separate cases are shown in Supplementary Fig. 2. The mean decrease in volume normalized to the initial volume in these seven cases comes to be 35 ± 11%.

The shrinkage of the nucleus as a function of time is plotted in Fig. 1 *C* (representative curves), as the change in the area of a confocal slice normalized to the area immediately after perturbation. Fig. 1 *D* shows the fractional nuclear shrinkage on perturbation of different regions (12 cells each). Notably, the shrinkage caused by perturbation at the heterochromatin is in many cases accompanied by an initial variable lag phase, followed by a sudden, apparently cooperative decay. Thus, to characterize the initial lag phase, we analyzed the 12 cases for which the statistics in Fig. 1 *D* had been calculated (the duration of the lag phase was regarded as the time required for a 5% decrease in the largest nuclear cross section after heterochromatin perturbation). The shortest of these times came to be 8 s (for the fast decays), and the longest ones were ~1 min in duration, before the inception of faster shrinkage. The mean time came out to be 36 ± 20 s. The initial lag phase in shrinkage suggests that the laser's effect is not a direct cutting of mechanical links at the point where the laser is applied but rather is a consequence of the cell's response to local heating of heterochromatin.

Perturbation at the envelope also caused nuclear shrinkage, but this is additionally accompanied by chromatin outflow at the perturbation spot. In contrast to perturbation of heterochromatin, nuclear envelope perturbation usually showed no lag times, and the nuclear size decreased faster. Importantly, similar experiments performed on fixed H2B-EGFP HeLa cells and on nuclei isolated from such cells showed negligible shrinkage (Fig. 1 *D*, statistics for 10 nuclei or cells). Typical images before and after perturbation for perturbation at the envelope and for isolated nuclei and fixed cells are presented in Supplementary Fig. 3.

Because the effect of the gold particles is only to make the local absorption of NIR radiation more efficient, it is reasonable to expect that similar effects might be observed at very high laser powers without the presence of the gold particles, and then the effects would be just because of cellular substructure and not the distribution of nanoparticles. Indeed, control cells without gold particles also showed shrinkage effects on heterochromatin perturbation by high laser powers (120–140 mW at the sample plane at a spot). At lower powers there is no effect beyond local photobleaching. The region-specific differential effect was present in the stated range of 120–140 mW in control cells. The results from these experiments are summarized in Supplementary Fig. 4.

Perturbation under various conditions that perturb chromatin

To further investigate the unusual shrinkage response of heterochromatin regions to gold-nanoparticle-mediated perturbation, we studied this response under various conditions that are known to modulate chromatin architecture. Typical images before and after perturbation under the above conditions are presented in Fig. 2 *A*. To probe whether the chromatin architecture was alone instrumental in nuclear organization and hence for the effect of shrinking on perturbation, HDACs

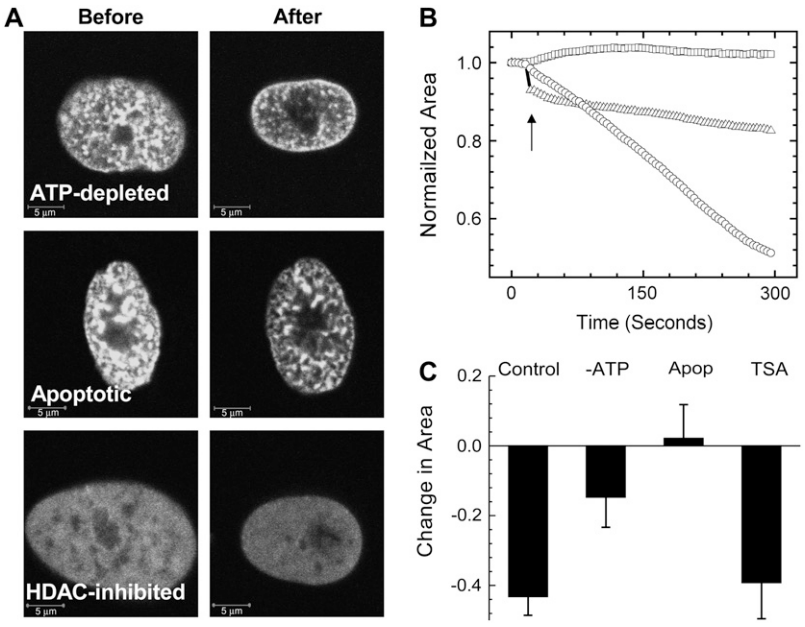

FIGURE 2 (*A*) Typical images before and after perturbation under different conditions of cellular perturbation: ATP depletion, staurosporine-induced apoptosis, and HDAC-inhibition by TSA. Scale bars are equal to 5 μm. (*B*) Representative plots of shrinkage dynamics under conditions of HDAC inhibition (*circles*), ATP depletion (*triangles*), and apoptosis (*squares*) on heterochromatin perturbation. A sharp decrease in area immediately on perturbation of ATP-depleted cells is indicated by the arrow. (*C*) Statistics of fractional change in area for perturbation under the different conditions indicated ($n = 12$), compared with shrinkage under conditions of heterochromatin perturbation in control cells ($n = 12$; from Fig. 1 *D*).

were inhibited by treatment with the drug trichostatin-A (TSA). HDAC inhibition leads to a widespread acetylation of the histone tails and thus decompacts the chromatin structure. Under these conditions, the H2B-EGFP fluorescence became largely uniform in ~3 h, with few relatively brighter patches corresponding to residual heterochromatin. Ablating the residual dense patches did not significantly alter the dynamics of nuclear shrinkage in comparison to heterochromatin perturbation in control cells. That chromatin decondensation by widespread histone acetylation does not affect the shrinkage dynamics probably is suggestive of an underlying scaffold providing mechanical stability to the nucleus in addition to chromatin structure. Next, we performed the heterochromatin perturbation experiments in ATP-depleted H2B-EGFP HeLa cells. Here the nuclear shrinkage dynamics was slowed down as compared to control cells (Fig. 2, *B* and *C*). A partial breakdown of the higher-order structure might be responsible for the slower shrinkage dynamics of the nuclei of ATP-depleted cells, indicating an active maintenance of cellular architecture. The slower shrinkage kinetics on ATP depletion does not necessarily mean that the shrinkage itself is an active process per se. A global perturbation such as this would affect both the chromatin assembly and the cytoplasmic anchors, and the net effect is what we monitor. Another condition of large-scale cellular perturbation is apoptosis, which is marked by condensation of chromatin and breakdown of higher-order structure by widespread cleavage of the DNA. Remarkably, however, with ablation of the condensed patches of chromatin in such cells, there was even a small but perceptible rise in the normalized area in cases (Fig. 2 *C*) accompanied by a smoothening out of the envelope.

Our data strongly lend support to a model of nuclear architecture where the heterochromatin is mechanically coupled to a scaffold underlying the nuclear envelope (12), whereas the euchromatin remains comparatively detached from such a proteinaceous skeleton. The perturbation-triggered shrinkage is reminiscent of a natural process in the cell cycle in which, at prophase, nuclear envelope breakdown brought about by invaginating microtubules is accompanied by a rapid decrease in nuclear volume as a result of chromatin condensation (11). A number of contacts among the nuclear lamina, envelope, and the cytoskeleton have been worked out (13,20). There have been suggestions that the interphase nucleus is held by a balance of opposing forces exerted by the chromatin and cytoplasmic filaments (11,21). This could also possibly account for the shrinkage on heterochromatin perturbation, via the disruption of a collection of cytoplasmic contacts. This could in turn lead to an imbalance of the forces and subsequently to nuclear collapse caused by an excess of inward forces. Then, as expected, the isolated nuclei devoid of the cytoplasmic anchors failed to show any further shrinkage on perturbation. The absence of a lag phase in the dynamics of nuclear collapse on envelope perturbation could correspond to a larger number of cytoplasmic contacts being disrupted.

Long-term effects of heterochromatin perturbation

To verify the state of the cell as a whole, we took DIC images of the cell along with fluorescence images of nuclear H2B-EGFP on heterochromatin perturbation. Interestingly, the shrinkage of the cell was not as remarkable as that of the nucleus. In some instances there appeared cytoplasmic connections to the nuclear membrane that were stretched until they subsequently broke, concomitant with nuclear shrinkage, as depicted in Fig. 3 *A*. This was followed by the appearance of plasma membrane blebs at later time points. Fig. 3 *B* shows the initiation of bleb formation at 10 min that became pronounced 20 min postperturbation. Thus, blebbing is probably not a direct effect of heating during the brief 3-s exposure to the NIR laser but is perhaps a downstream effect of signaling cascades initiated by the cell in response to perturbation. At still later time points, cell death sets in on the perturbed cells as observed by a fragmentation of the chromatin indicated by H2B-EGFP fluorescence, as shown in Fig. 3 *C*, where most of the cells in the field of view were perturbed at the heterochromatin. Further evidence for early apoptosis is presented in Supplementary Fig. 5.

State of nuclear and cytoplasmic filaments on heterochromatin perturbation

Lamin B1 is a vital structural protein in the cell nucleus. We find that on heterochromatin perturbation the lamin scaffold does not depolymerize and undergoes shrinkage concomitant with nuclear collapse. This is depicted in Fig. 4, *A* and *B*, where simultaneous confocal imaging of EGFP-lamin B1 and linker histone H1e-mRFP as chromatin marker are shown. Next we sought to verify the state of cytoplasmic filaments on perturbation. Actin stress fibers do not seem to depolymerize as visualized by actin-EGFP. However, the network of stress fibers seems to shrink, giving rise to pronounced blebs at the distal edges of the cell (Fig. 4 *C*). To determine whether the mechanical response on heterochromatin perturbation transduces down to the focal adhesion points through which cells mechanically interact with the extracellular matrix/substrate, we fixed and stained such heterochromatin-perturbed cells for paxillin as a focal adhesion point marker, and actin. Here the perturbed and control cells were imaged in the same plate. Remarkably we found that, although as before the actin stress fibers did not depolymerize, the paxillin staining at the focal adhesion points vanished entirely from the heterochromatin-perturbed cells, showing that the mechanical response to nuclear shrinkage can be found down to these distal nodes. A representative image is presented in Fig. 4 *D*. Of the three nuclei seen, the one on the right has been perturbed at heterochromatin; the other two serve as controls. Because the image is close to the lower plasma membrane and the nuclei are at a higher *z*-plane, they appear slightly defocused.

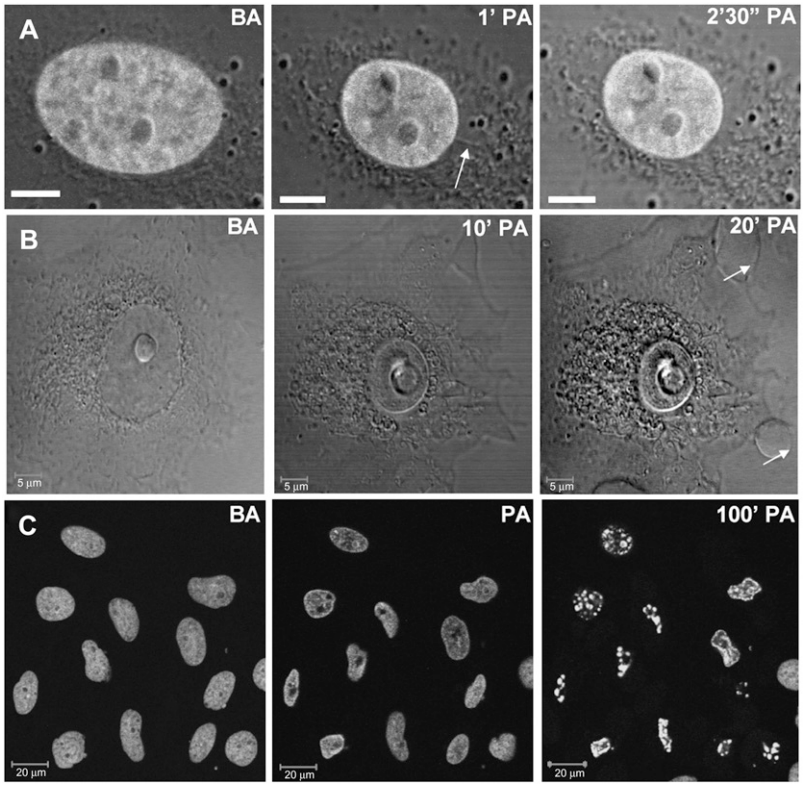

FIGURE 3 In all images, BA indicates ''before perturbation'', and PA ''postperturbation''. (*A*) Presence of cytoplasmic filaments (*arrow*) seen through time-lapse fluorescence-DIC images under conditions of heterochromatin perturbation. Scale bars are equal to 5 μm. (*B*) Time lapse DIC images to show that membrane blebs (*arrows*) appear at later time points on perturbation. (*C*) Chromatin fragmentation caused by subsequent apoptosis seen in fluorescence time-lapse images of a field of heterochromatin-perturbed cells. Scale bars are equal 20 μm. The time indicated in *C* is only approximate, as the cells were perturbed individually, and different cells are at different stages of progression toward cell death. Time points are indicated at the top of each picture.

Transiently transfected τ-EGFP, which is a microtubule-associated protein, on the other hand, becomes diffused on heterochromatin perturbation (Fig. 4 *E*). To verify the state of microtubule and vimentin (an intermediate filament) organization, we stained the perturbed cells with antibodies to α-tubulin and vimentin (Fig. 4, *F* and *G*). In keeping with the homogenizing of the τ-EGFP, microtubules indeed become fragmented, but in contrast, the intermediate filament structure remains intact. As before, the perturbed and control cells were imaged in the same plate.

A possible role of cytoplasmic players and chromatin state is also seen in the different nuclear sizes under the various conditions tested (Supplementary Fig. 6). Isolated nuclei taken out of the cytoplasmic milieu are more spherical in shape and are ~50% the size of nuclei in living cells. Notably this is also the approximate size that nuclei of heterochromatin-perturbed GI cells shrink to. Interestingly the isolated nuclei failed to show any further shrinkage on perturbation. There have been suggestions that chromatin in interphase cells are like taut springs anchored to a perinuclear substrate (11). In isolated nuclei it is likely that these springs have already collapsed to their resting lengths, thus resulting in negligible shrinkage on perturbation. To verify the state of the nuclear pores on perturbation, we transiently transfected HeLa cells with the transcriptional coactivator Activated Notch1 tagged with EGFP and the linker histone H1e-mRFP as a chromatin marker. Although, the more chromatin-bound H1e-mRFP did not disperse significantly, Activated Notch-EGFP did indeed leak out into the cytoplasm (Supplementary Fig. 7), suggesting the loss of nuclear envelope integrity on perturbation, although from this experiment it is not possible to delineate whether this is by a disruption of the nuclear membrane or the pore complexes. Cytoplasmic perturbation also leads to nuclear shrinkage (Fig. 5), suggesting again the role of the balance of forces stabilizing the shape and size of nuclei in intact cells. A schematic of the cellular and nuclear response to gold-nanoparticle-assisted laser perturbation of heterochromatin assembly is depicted in Fig. 6.

DISCUSSION

Advances in genetic, biochemical, and imaging techniques have given much of our current understanding on structure, dynamics, and function inside the eukaryotic cell nucleus. However, visualization of static or dynamic states of the cell in conjunction with attempts to actively perturb subcellular structures, using laser microsurgery, has begun to provide possibilities of regional perturbation and facile genetic manipulation in single cells. Such methods in the past have been used to study embryos of organisms such as *C. elegans* (22) and *Drosophila melanogaster*(23,24) and even to manipulate the mitotic spindle in small yeast cells (25). Perturbation of specific cellular substructures is also now possible, as demonstrated by the disruption of individual microtubule filaments (26) and actin stress fibers (27).

The cellular response of a cell to nanoparticle-mediated perturbation shows a stark difference depending on whether the heterochromatin or the euchromatin is perturbed. This

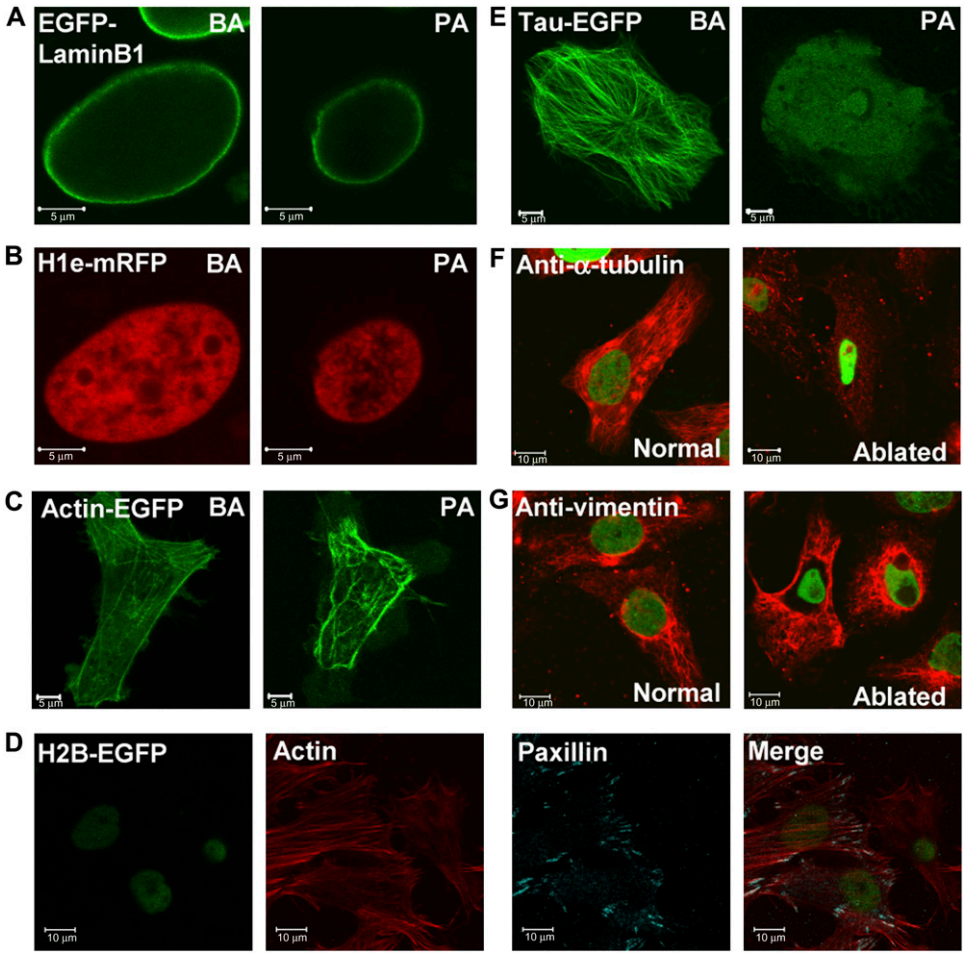

FIGURE 4 State of the nuclear lamin on heterochromatin perturbation. HeLa cells were cotransfected with (*A*) EGFP-Lamin B1 and (*B*) H1e-mRFP. Images before and after perturbation are presented for the same cell. (*C*) Images of HeLa cells transiently transfected with Actin-EGFP before and after heterochromatin perturbation. Heterochromatin was identified by Hoechst staining of the DNA in these cases (images not shown). (*D*) H2B-EGFP-expressing HeLa cells were perturbed at the heterochromatin, fixed, and stained with an antibody against paxillin (visualized by a Cy5-labled secondary antibody) and filamentous actin bound by an Alexa-568–labeled phalloidin. Individual and merged images are presented. (*E*) Images of HeLa cells transiently transfected with Tau-EGFP as a microtubule marker before and after heterochromatin perturbation. As in *C*, heterochromatin was identified by Hoechst staining of the DNA. Images of H2B-EGFP expressing HeLa cells perturbed at the heterochromatin and stained with primary antibodies against (*F*) α-tubulin and (*G*) vimentin on separate plates. A Cy3-labled secondary antibody was used. Normal and perturbed cells were imaged on the same plate. Green indicates H2B-EGFP fluoresecnce, whereas red shows the respective cytoplasmic filaments. Scale bars are equal to 5 μm in *A*, *B*, *C*, and *E*. Scale bars are equal to 10 μm in *D*, *F*, and *G*.

suggests that the heterochromatin may be mechanically linked to a scaffold vital for nuclear organization. This is further probed under conditions that affect chromatin structure differently such as HDAC inhibition, ATP depletion, and staurosporine-induced apoptosis. Shrinkage kinetics on heterochromatin perturbation was largely unaffected on HDAC inhibition, indicating the role of a possible underlying proteinaceous scaffold in maintaining nuclear architecture. However, ATP-depleted cells showed slower nuclear shrinkage on perturbation. Despite an initial collapse during the 3 s of irradiation, the subsequent shrinkage is slower because ATP depletion affects a variety of parameters such as the exchange rates of core histones, the overall higher-order structure of the chromatin, and the cytoplasmic filaments. Apoptosis affects cellular structures more drastically, and chromatin is both condensed and fragmented. In apoptotic nuclei, a contrasting mechanical response was elicited on perturbation, with nuclei showing even a minor expansion in a number of cases.

The possible role of cytoplasmic tethers and long-term effects of perturbation are also described. Isolated nuclei are consistently smaller than nuclei in cells, indicating that the chromatin is held partially open against the compacting forces of histone tail interactions in intact cells. Some of these tethers are seen to rupture during the shrinkage process, but their exact identity is yet to be determined. As might be

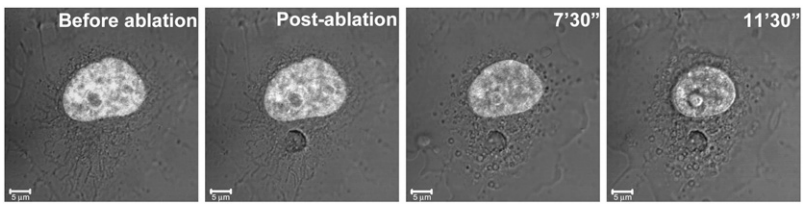

FIGURE 5 Nuclear shrinkage and cytoplasmic blebs at late time points are also seen on cytoplasmic perturbations (scale bar = 5 μm). Fluorescence image of the nucleus of an H2B-EGFP HeLa cell is overlaid on a transmission DIC image. Time points are indicated at the top.

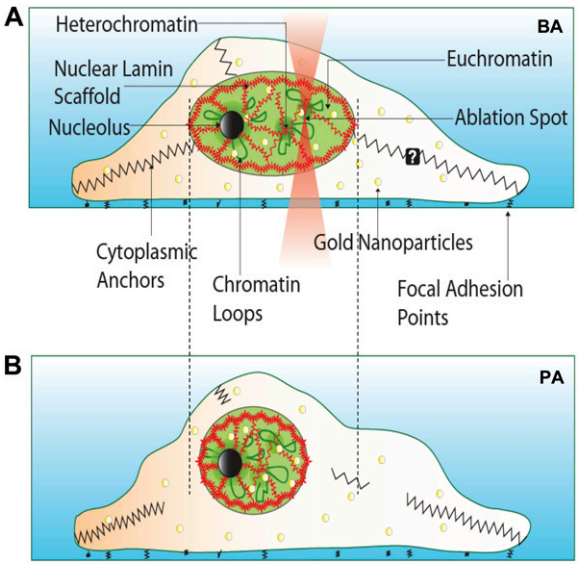

FIGURE 6 Model for the maintenance of cell nuclear architecture. (*A*) The nucleus is held under opposing tensions because of the chromatin and cytoplasmic filaments. On shining of an infrared laser on gold nanoparticle (*yellow circles*)-incorporated cells at the heterochromatin, there is a breaking of cytoplasmic contacts, resulting in a collapse of the nuclear volume depicted in *B*. The underlying lamin scaffold undergoes concomitant shrinkage but does not disintegrate during this process.

expected, cytoplasmic perturbation also leads to nuclear shrinkage (Fig. 5).

In summary, we describe a novel nanoparticle-assisted NIR-based laser perturbation method to perturb cellular substructure in a controlled manner. Using this method, we have explored the interplay between the chromatin assembly and the nuclear architecture in the eukaryotic cell. Our findings reveal a highly interconnected mechanical organization depicting heterochromatin as forming vital nodes for the maintenance of nuclear architecture. Perturbations of these nodes reveal its direct differential coupling to specific cytoskeletal network elements.

SUPPLEMENTARY MATERIAL

To view all of the supplemental files associated with this article, visit www.biophysj.org.

We thank the National Centre for Biological Sciences imaging facility and the National Nanoscience Initiative, Department of Science & Technology, India, for financial assistance.

REFERENCES

1. Cremer, T., and C. Cremer. 2001. Chromosome territories, nuclear architecture and gene regulation in mammalian cells. *Nat. Rev. Genet.* 2:292–301.
2. Foster, H. A., and J. M. Bridger. 2005. The genome and the nucleus: a marriage made by evolution. Genome organisation and nuclear architecture. *Chromosoma.* 114:212–229.
3. Horowitz-Scherer, R. A., and C. L. Woodcock. 2006. Organization of interphase chromatin. *Chromosoma.* 115:1–14.
4. Kosak, S. T., and M. Groudine. 2004. Gene order and dynamic domains. *Science.* 306:644–647.
5. Gerlich, D., J. Beaudouin, B. Kalbfuss, N. Daigle, R. Eils, and J. Ellenberg. 2003. Global chromosome positions are transmitted through mitosis in mammalian cells. *Cell.* 112:751–764.
6. Parada, L. A., P. G. McQueen, and T. Misteli. 2004. Tissue-specific spatial organization of genomes. *Genome Biol.* 5:R44.1–R44.9.
7. Sproul, D., N. Gilbert, and W. A. Bickmore. 2005. The role of chromatin structure in regulating the expression of clustered genes. *Nat. Rev. Genet.* 6:775–781.
8. Zaidi, S. K., D. W. Young, J. Y. Choi, J. Pratap, A. Javed, M. Montecino, J. L. Stein, A. J. van Wijnen, J. B. Lian, and G. S. Stein. 2005. The dynamic organization of gene-regulatory machinery in nuclear microenvironments. *EMBO Rep.* 6:128–133.
9. Osborne, C. S., L. Chakalova, K. E. Brown, D. Carter, A. Horton, E. Debrand, B. Goyenechea, J. A. Mitchell, S. Lopes, W. Reik, and P. Fraser. 2004. Active genes dynamically colocalize to shared sites of ongoing transcription. *Nat. Genet.* 36:1065–1071.
10. Gilbert, N., S. Boyle, H. Fiegler, K. Woodfine, N. P. Carter, and W. A. Bickmore. 2004. Chromatin architecture of the human genome: gene-rich domains are enriched in open chromatin fibers. *Cell.* 118: 555–566.
11. Beaudouin, J., D. Gerlich, N. Daigle, R. Eils, and J. Ellenberg. 2002. Nuclear envelope breakdown proceeds by microtubule-induced tearing of the lamina. *Cell.* 108:83–96.
12. Labrador, M., and V. G. Corces. 2002. Setting the boundaries of chromatin domains and nuclear organization. *Cell.* 111:151–154.
13. Gruenbaum, Y., A. Margalit, R. D. Goldman, D. K. Shumaker, and K. L. Wilson. 2005. The nuclear lamina comes of age. *Nat. Rev. Mol. Cell Biol.* 6:21–31.
14. Haithcock, E., Y. Dayani, E. Neufeld, A. J. Zahand, N. Feinstein, A. Mattout, Y. Gruenbaum, and J. Liu. 2005. Age-related changes of nuclear architecture in *Caenorhabditis elegans*. *Proc. Natl. Acad. Sci. USA.* 102:16690–16695.
15. Goldman, R. D., D. K. Shumaker, M. R. Erdos, M. Eriksson, A. E. Goldman, L. B. Gordon, Y. Gruenbaum, S. Khuon, M. Mendez, R. Varga, and F. S. Collins. 2004. Accumulation of mutant lamin A causes progressive changes in nuclear architecture in Hutchinson-Gilford progeria syndrome. *Proc. Natl. Acad. Sci. USA.* 101:8963–8968.
16. Tamada, M., M. P. Sheetz, and Y. Sawada. 2004. Activation of a signaling cascade by cytoskeleton stretch. *Dev. Cell.* 7:709–718.
17. Zink, D., A. H. Fischer, and J. A. Nickerson. 2004. Nuclear structure in cancer cells. *Nat. Rev. Cancer.* 4:677–687.
18. Koberna, K., D. Stanek, J. Malinsky, M. Eltsov, A. Pliss, V. Ctrnacta, S. Cermanova, and I. Raska. 1999. Nuclear organization studied with the help of a hypotonic shift: its use permits hydrophilic molecules to enter into living cells. *Chromosoma.* 108:325–335.
19. Shukla, R., V. Bansal, M. Chaudhary, A. Basu, R. R. Bhonde, and M. Sastry. 2005. Biocompatibility of gold nanoparticles and their endocytotic fate inside the cellular compartment: a microscopic overview. *Langmuir.* 21:10644–10654.
20. Houben, F., F. C. Ramaekers, L. H. Snoeckx, and J. L. Broers. 2007. Role of nuclear lamina-cytoskeleton interactions in the maintenance of cellular strength. *Biochim. Biophys. Acta.* 1773:675–686.
21. Maniotis, A. J., C. S. Chen, and D. E. Ingber. 1997. Demonstration of mechanical connections between integrins, cytoskeletal filaments, and nucleoplasm that stabilize nuclear structure. *Proc. Natl. Acad. Sci. USA.* 94:849–854.
22. Grill, S. W., P. Gonczy, E. H. Stelzer, and A. A. Hyman. 2001. Polarity controls forces governing asymmetric spindle positioning in the *Caenorhabditis elegans embryo*. *Nature.* 409:630–633.
23. Schmucker, D., A. L. Su, A. Beermann, H. Jackle, and D. G. Jay. 1994. Chromophore-assisted laser inactivation of patched protein switches

cell fate in the larval visual system of *Drosophila*. *Proc. Natl. Acad. Sci. USA*. 91:2664–2668.

24. Supatto, W., D. Debarre, B. Moulia, E. Brouzes, J. L. Martin, E. Farge, and E. Beaurepaire. 2005. In vivo modulation of morphogenetic movements in *Drosophila* embryos with femtosecond laser pulses. *Proc. Natl. Acad. Sci. USA*. 102:1047–1052.
25. Carvalho, P., and D. Pellman. 2004. Mitotic spindle: laser microsurgery in yeast cells. *Curr. Biol.* 14:R748–R750.
26. Botvinick, E. L., V. Venugopalan, J. V. Shah, L. H. Liaw, and M. W. Berns. 2004. Controlled ablation of microtubules using a picosecond laser. *Biophys. J.* 87:4203–4212.
27. Kumar, S., I. Z. Maxwell, A. Heisterkamp, T. R. Polte, T. P. Lele, M. Salanga, E. Mazur, and D. E. Ingber. 2006. Viscoelastic retraction of single living stress fibers and its impact on cell shape, cytoskeletal organization, and extracellular matrix mechanics. *Biophys. J.* 90:3762–3773.